Closed-loop Stiffness and Damping Accuracy of Impedance-type Haptic Displays

Nick Colonnese* Sean M. Sketch† Allison M. Okamura‡

Department of Mechanical Engineering, Stanford University

ABSTRACT

Impedance-type kinesthetic haptic displays aim to render arbitrary desired dynamics to a human operator using force feedback. To effectively render realistic virtual environments, the difference between desired and rendered dynamics must be small. In this paper, we analyze the closed-loop dynamics of haptic displays for three common virtual environments: a spring, a damper, and a spring-damper, including the effects of time delay and low-pass filtering. Using a linear model, we identify important parameters for accuracy in terms of "effective impedances," a conceptual tool that decomposes the display's closed-loop impedance to components with physical analogs. Our results establish bandwidth limits for rendering effective stiffness and damping. The stiffness bandwidth is limited by the virtual stiffness and device mass, and the damping bandwidth is limited by the cut-off frequency of the low-pass filter. Time delay reduces the effective damping of spring and spring-damper displays, reduces the effective mass for damper displays, and can introduce effective jerk feedback; otherwise delay has negligible effect on accuracy (when the system is stable). Experimental data gathered with a Phantom Premium 1.5 validates the theoretical analysis. This work informs haptic display design by presenting how closed-loop behavior changes with key parameters.

Index Terms: L.2.0.a [Haptics]: Kinesthetic devices; L.2.0.o [Haptics]: Transparency; L.2.0.u [Haptics] System design and analysis.

1 INTRODUCTION

Impedance-type kinesthetic haptic displays are composed of (1) a device equipped with sensors and actuators that provides force feedback to the user and (2) a rendering algorithm that computes force feedback as a function of device motion (Figure 1). Given a map from sensed position to actuator force (i.e., a virtual environment), the display is characterized by its closed-loop impedance, which describes the frequency-dependent relationship between input position and output force. The objective of accurate haptic rendering is to manipulate the rendered impedance of these displays to match a desired impedance through mechanical and feedback control design. Accurate haptic displays should feel exactly as desired, with no unwanted effects from a multitude of sources such as device dynamics (i.e., inherent inertia and friction), analog to digital (A/D) and digital to analog (D/A) conversions, aggressive low-pass filtering to mitigate noise, and amplifier or transport time delay. In addition to featuring the desired input-output characteristics, high-performance haptic displays must be stable and insensitive to noise. Past research has established rigorous conditions concerning stability and noise characterization. However, current results for haptic display accuracy are not complete. Characterization of the effect of system parameters (e.g., device mass, programmed virtual environment structure and parameters, and time delay) on the closed-loop impedance would be a valuable tool in haptic display design. The characterization in this paper is particularly relevant for closed-loop display of stiffness and damping.

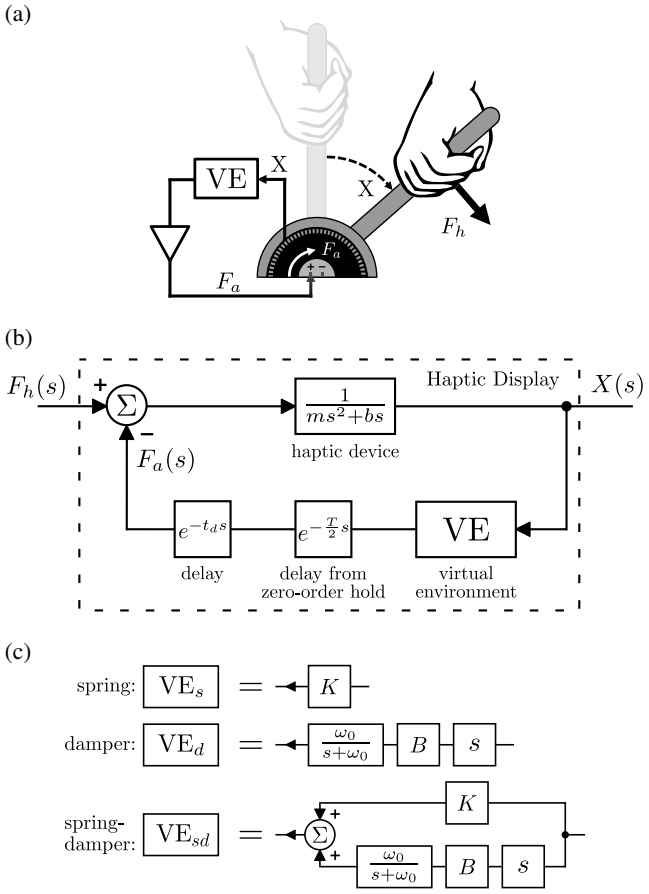

Figure 1: (a) Schematic of a human interacting with a haptic device implementing a virtual environment. (b) Block diagram for this system. (c) The different types of virtual environments: spring, damper, or spring-damper.

This work builds on previous research on the accuracy of kinesthetic haptic displays and teleoperated systems. Analyzing the performance of a haptic system based on its input-output properties is similar to analyzing the "transparency" of a teleoperated system. For such systems, greater transparency translates to closer force and position signal matching between master and slave devices [8]. Lawrence et al. experimentally explored transparency in haptic displays by investigating the ability of humans to detect differences in mechanical impedances [9]. McJunkin et al. performed a similar experiment with a different scope by comparing the transparency bandwidth of a haptic display with both active (human input) and

*ncolonnese@stanford.edu
†ssketch@stanford.edu
‡aokamura@stanford.edu

IEEE Haptics Symposium 2014
23-26 February, Houston, Tx, USA
978-1-4799-3131-6/14/$31.00 ©2014 IEEE

passive (motor driven) interaction tests [11]. In both of the studies, the experimental closed-loop behavior of the displays was analyzed. However, no theoretical models of how closed-loop behavior changes with system parameters were established.

Griffiths et al. define a notion of accuracy for impedance-type haptic displays called "distortion," which is similar to transparency. Distortion is the frequency-dependent difference between actual and desired closed-loop dynamics, normalized by the desired dynamics [5]. The concept is useful for elucidating abstract trade-offs in haptic design. However, because distortion does not analyze the closed-loop impedance directly, using it to identify the effect of system parameters can be difficult. Griffiths et al. did not directly analyze how distortion depends on time delay or low-pass filtering; both could affect the impedance of the display.

In this paper, we address haptic accuracy by analyzing the closed-loop dynamics of haptic displays for three common virtual environments: a spring, a viscous damper, and a spring-damper. We include the effects of time delay and low-pass filtering. These environments are ubiquitous in practice for rendering "hard" surfaces, and are the building blocks for more complex virtual environments. In each case, we identify the important parameters for accuracy by decomposing the closed-loop impedance to "effective impedances." Effective impedances present the same information as other frequency response tools, such as Bode or Nyquist plots, but more intuitively express the system response through their physical analogs.

Our results, given in terms of effective impedances, demonstrate that spring and spring-damper haptic displays render a nonzero effective stiffness only up to $\omega_s^* = \sqrt{K/m}$, where K represents the virtual stiffness, and m the device mass. Damper and spring-damper displays render the desired effective damping up to the cut-off frequency of the low-pass filter $\omega_b^* = \omega_0$. As long as the system is stable, time delay reduces the effective damping of spring and spring-damper displays, reduces the effective mass for pure damper displays, and can introduce effective jerk feedback.

Experimental data was gathered to model a Phantom Premium 1.5 haptic device. The Premium was then used to compare experimental and theoretical closed-loop frequency responses for each virtual environment. This work informs the design of haptic displays by modeling how closed-loop behavior (in terms of effective impedances) is affected by system parameters and time delay.

2 System Models

In this section we introduce system models for a human interacting with a 1-degree-of-freedom (1-dof) haptic device rendering virtual environments, and also present the concept of effective impedances. The system models are used to generate theoretical closed-loop impedances for haptic displays. Effective impedances show a closed-loop frequency response in terms of physical analogs to communicate how a haptic display "feels."

2.1 System Model

Figure 1 gives a schematic and block diagram for the system model. The haptic device is modeled as a mass m with viscous damping b. We analyze three virtual environments (VEs), that map sensed position to actuator forces: a spring, a damper, and a spring-damper consisting of a spring and damper in parallel. These virtual environments were chosen for their ubiquity in rendering "hard" dynamics in practice (e.g., a virtual wall), as well as for their simplicity. The damper feedback requires a differentiation of sensed position. Because differentiation amplifies high-frequency noise, the velocity estimate is low-pass filtered with a unity gain filter at zero frequency and a cut-off frequency of ω_0 (rad/s). Linear, continuous models are used for the straightforward application of frequency response tools. To account for the fact that control is performed through a computer containing A/D and D/A components, a time

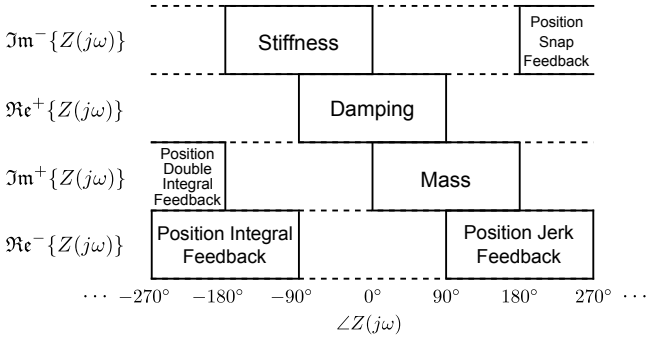

Figure 2: Effective impedances are defined for both signs of the real and imaginary components of $Z(j\omega)$, and its angle $\angle Z(j\omega)$. For most haptic displays, where $-90° \le \angle Z(j\omega) \le 90°$, effective stiffness, damping, and mass, are the only nonzero effective impedances.

delay of half the sample time is included in the feedback loop. In addition to this inherent system delay, there is also an external time delay t_d resulting from potential amplifier or transport delay.

2.2 Effective Impedances

To aid the analysis of these haptic displays, we show frequency response information as effective impedances. This approach has been previously used to describe effective damping and mass [12]. For a transfer function representing the impedance of a system, $Z(s) = F(s)/V(s)$, the effective impedances are defined as

$$\vdots$$

$$\begin{aligned}
\text{Eff. Integral FB} &= EIF(\omega) = \omega^2 \mathfrak{Re}^-\{Z(j\omega)\} && -270° \le \theta \le -90°,\\
\text{Eff. Stiffness} &= ES(\omega) = \omega \mathfrak{Im}^-\{Z(j\omega)\} && -180° \le \theta \le 0°,\\
\text{Eff. Damping} &= ED(\omega) = \mathfrak{Re}^+\{Z(j\omega)\} && -90° \le \theta \le 90°,\\
\text{Eff. Mass} &= EM(\omega) = \omega^{-1} \mathfrak{Im}^+\{Z(j\omega)\} && 0° \le \theta \le 180°,\\
\text{Eff. Jerk FB} &= EJF(\omega) = \omega^{-2} \mathfrak{Re}^-\{Z(j\omega)\} && 90° \le \theta \le 270°,
\end{aligned}$$

$$\vdots$$

where FB is an abbreviation for feedback and $\theta = \angle Z(j\omega)$. The vertical dots show that effective impedances are defined for any $\angle Z(j\omega)$. This presentation of the frequency response decomposes the system impedance into some components that coincide with physical analogs. For example, effective stiffness is the component of the force in phase with position. Some effective impedances, e.g., jerk and higher derivatives of position feedback, do not have simple mechanical analogs. Figure 2 shows a chart of the phase of $Z(j\omega)$ and the corresponding effective impedances for real and imaginary components. For the analysis performed on the virtual environments presented here, effective stiffness, damping, and mass are most relevant.

Figure 3 displays Nyquist and effective impedance plots for a sample system with impedance

$$Z(s) = \frac{F(s)}{V(s)} = \frac{s^2 + 20s + 100}{100s}. \tag{1}$$

This particular sample impedance is chosen because it is similar to the closed-loop display impedances analyzed.

3 Environments

In this section we analyze the closed-loop dynamics of haptic displays with and without time delay for spring, viscous damper, and

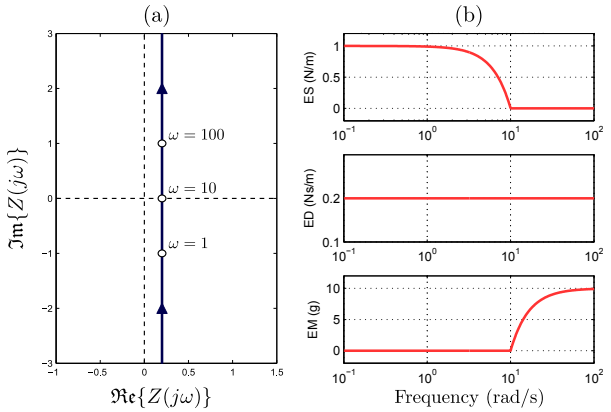

Figure 3: (a) Nyquist plot displaying the frequency response of the sample system $Z(j\omega)$ given in Equation (1). (b) The effective stiffness (ES), damping (ED), and mass (EM), of $Z(j\omega)$; all other effective impedances are zero at all frequencies.

spring-damper virtual environments. For a given virtual environment, the display's closed-loop impedance is

$$\frac{F_h(s)}{V(s)} = Z(s) = \frac{1 + G_d[\mathrm{VE}e^{-j\omega(T/2+t_d)}]}{G_d s}, \tag{2}$$

where G_d represents the position to force transfer function of the haptic device,

$$G_d = \frac{1}{ms^2 + bs}. \tag{3}$$

The mass and viscous damping of the haptic device used to generate Figures 4-8 are $m = 100$ (g), and $b = 0.1$ (Ns/m). These values were chosen to be representative of existing impedance-type haptic devices [2]. Our analysis will identify symbolic expressions for (1) the effective stiffness bandwidth, (2) the effective damping bandwidth, (3) the relationship between reduction in effective damping and time delay, and (4) the relationship between reduction in effective mass and time delay. Numerical values are used only for quantitative plotting.

3.1 Spring

The closed-loop impedance of a haptic display rendering a spring is

$$Z_s(s) = \frac{ms^2 + bs + Ke^{-j\omega(T/2+t_d)}}{s}. \tag{4}$$

The numerator of $Z_s(s)$ is a classic second-order system, except for a linear-in-frequency phase delay on K, which depends on the sample time T and external delay t_d. The Bode and effective impedance plots for this system are shown in Figure 4 with varying amounts of total time delay $(T/2+t_d)$.

For parameter values in which the system is stable [3], its frequency response has a magnitude close to K/ω and a phase of -90° up to a critical frequency,

$$\omega_s^* = \sqrt{\frac{K}{m}}. \tag{5}$$

The resonance peak at ω_s^* and frequency span for which the phase of the system changes from -90° to 90° depends on device damping *and* the total time delay.

It can be difficult to intuit how a spring haptic display "feels" from the magnitude and phase given by a Bode plot. To aid interpretation, we also present the closed-loop display effective impedances. For frequencies less than ω_s^*, the display has effective stiffness, ES, of K, and effective mass, EM, of zero. For frequencies larger than ω_s^*, ES is zero, and EM tends to the device

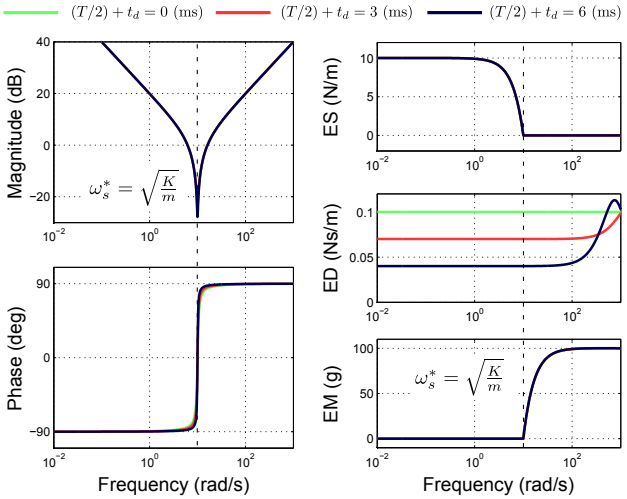

Figure 4: Spring VE Bode and effective impedance plots with K = 10 (N/m) and varying amounts of total delay. The displays have an ES close to K up to the effective stiffness bandwidth at $\omega_s^* = \sqrt{K/m}$, after which, ES drops to zero and EM dominates. Delay reduces ED by $K(T/2+t_d)$, but does not significantly affect ES or EM.

mass. The desired dynamics of a spring haptic display is a constant stiffness across all frequencies. Because the actual spring display renders a nonzero ES only up to ω_s^*, the ES bandwidth is defined by Equation (5). With no delay, the effective damping, ED, is constant across all frequencies at the device damping b. Adding delay to the system *decreases* ED by $K(T/2+t_d)$ for lower frequencies relevant to haptic accuracy. ED tends to the device damping at higher frequency. Because ED decreases by $K(T/2+t_d)$, negative ED is predicted for $b < K(T/2+t_d)$. Interestingly, this inequality, which describes conditions for negative ED, also describe the stability boundary for a spring virtual environment obtained using the Nyquist criterion [3]. Unlike ED, ES and EM are not significantly affected by delay; instability arises before delay can affect them.

3.2 Viscous Damper

The impedance of a closed-loop display rendering a damper is

$$Z_d(s) = \frac{ms^2 + (m\omega_0 + b)s + (b + Be^{-j\omega(T/2+t_d)})\omega_0}{s + \omega_0}. \tag{6}$$

The system has two zeros from a second-order system, and a pole at $-\omega_0$, along with delay on virtual damping B. System behavior depends on how the cut-off frequency of the low-pass filter, ω_0, compares to $\bar{\omega} = (b+B)/m$, which represents a pole of the damper display with no low-pass filter. If $\omega_0 \gg \bar{\omega}$, then the second-order system in the numerator of $Z_d(s)$ is overdamped, with one zero close to $\bar{\omega}$ and another at a high frequency not relevant to accuracy. If $\omega_0 \ll \bar{\omega}$, then the second-order system is underdamped. The Bode and effective impedance plots of the damper closed-loop displays are shown in Figure 5 with no delay for three conditions: (1) $\omega_0 \ll \bar{\omega}$, (2) $\omega_0 \approx \bar{\omega}$, (3) $\omega_0 \gg \bar{\omega}$.

For no delay, when the system is stable, the ED is the sum of the device and virtual damping, $(b+B)$, for frequencies less than ω_0, and just the device damping, b, for higher frequencies. Because the display renders the desired ED only up to ω_0, the ED bandwidth is defined by ω_0, $\omega_b^* = \omega_0$. The lower ω_0 is with respect to $\bar{\omega}$, the EM is reduced from the device mass for frequencies less than ω_0; when $\omega_0 \ll \bar{\omega}$, corresponding to aggressive filtering, EM is zero and the damper system has nonzero ES. EM tends to the device mass for frequencies after ω_0.

Figure 6 displays the Bode and effective impedance plots for the damper displays when $\omega_0 \gg \bar{\omega}$ with varying levels of delay. Adding

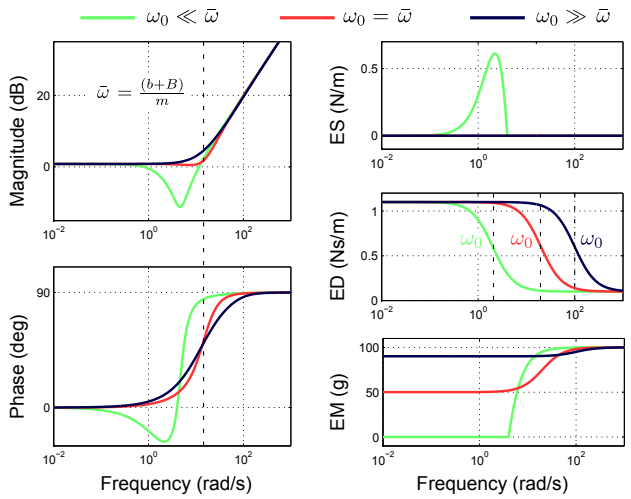

Figure 5: Damper VE Bode and effective impedance plots with B = 1 (Ns/m) and varying values of cut-off frequency ω_0. The effective damping bandwidth is ω_0. The colored ω_0 represents the distinct cut-off frequencies for the three systems. As ω_0 is reduced, corresponding to more aggressive filtering, EM and the ED bandwidth are reduced. When $\omega_0 < \bar{\omega} = (b+B)/m$, the system has nonzero ES.

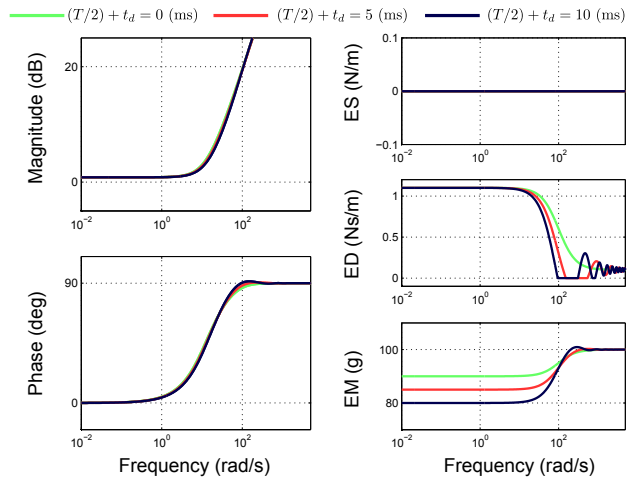

Figure 6: Damper VE Bode and effective impedance plots with B = 1 (Ns/m) and varying delay for $\omega_0 \gg \bar{\omega} = (b+B)/m$. Increasing delay reduces the ED bandwidth. EM is reduced by $B(T/2+t_d)$ from its no-delay value at low frequencies.

delay to the system affects its closed-loop impedance in two ways. First, delay reduces EM from the no-delay value by $B(T/2+t_d)$. This is similar to delay reducing ED in the spring environment by $K(T/2+t_d)$. Second, delay reduces ED bandwidth, and introduces oscillations in ED for frequencies past ω_0. These oscillations can introduce nonzero effective jerk feedback, EJF, at some frequencies.

3.3 Spring-Damper

The closed-loop impedance of display rendering a spring-damper is

$$Z_{sd}(s) = \frac{ms^3 + (m\omega_0 + b)s^2 + [b\omega_0 + (B\omega_0 + K)d]s + K\omega_0 d}{s(s+\omega_0)}, \tag{7}$$

where

$$d = e^{-j\omega(T/2+t_d)}. \tag{8}$$

The Bode and effective impedance plots of the spring-damper displays are shown in Figure 7 with no delay for three different cut-off

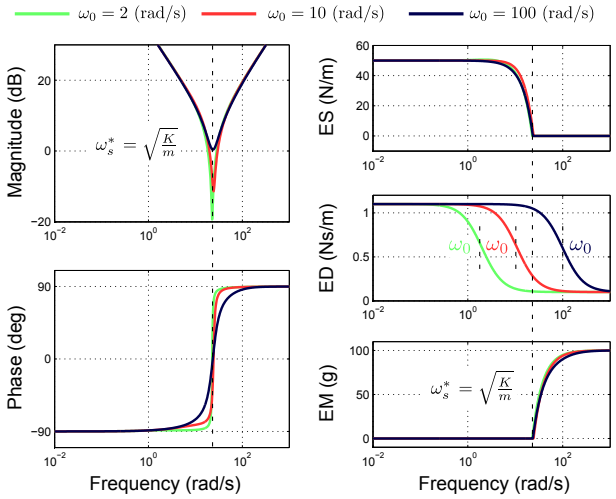

Figure 7: Spring-damper VE Bode and effective impedance plots with K = 50 (N/m), B = 1 (Ns/m), and varying values of the cut-off frequency ω_0. The systems have an ES of K up to the bandwidth of the system at $\omega_s^* = \sqrt{K/m}$, after which the ES drops to zero and the EM dominates. As ω_0 is reduced, so is the frequency span for which the ED is $(b+B)$.

frequencies. Like the pure spring display, the magnitude of the frequency response is close to K/ω and the phase is -90° for frequencies less than ω_s^*. The resonance peak at ω_s^* and frequency span for which the phase of the system changes from -90° to 90° depends on the *effective* damping (in contrast to the device damping as was the case for the spring environment) and total time delay. For frequencies less than ω_s^*, the display has an ES of K, and an EM of zero. For frequencies larger than ω_s^*, ES is zero, and EM tends to the device mass. The ED is the sum of the device and virtual damping, $(b+B)$, for frequencies less than ω_0, and just the device damping, b, for frequencies larger. These results establish that the spring-damper display has an ES bandwidth given by Equation (5), and an ED bandwidth of the cut-off frequency ω_0.

Delay affects the spring-damper display much like it does for the pure spring and damper environments. Figure 8 presents the Bode and effective impedance plots for the spring-damper with varying levels of delay. Adding delay reduces ED by $K(T/2+t_d)$ for frequencies less than ω_0 and also introduces oscillations in ED (which can introduce nonzero EJF at some frequencies), for frequencies past ω_0.

4 Experiments

Experiments were conducted with a Phantom Premium 1.5 to compare experimental data to theoretical predictions. These experiments were performed on a single joint of the device (the first revolute joint). The other degrees of freedom were mechanically constrained by a custom made fixture (Figure 9). Two types of experiments were performed. The first used system identification to find the device properties. The second determined the closed-loop impedances, or experimental transfer function estimates (ETFEs), of the spring-damper haptic displays.

4.1 System Identification of Haptic Device Properties

A time-based system identification procedure was used to determine open-loop properties (mass and viscous damping) of the Phantom Premium 1.5.

Ideally, at every instant in time the system should satisfy

$$f(t) = \hat{m}\ddot{x}(t) + \hat{b}\dot{x}(t), \tag{9}$$

where $f(t)$ is the external force, $\ddot{x}(t)$ and $\dot{x}(t)$ are the acceleration and velocity of the device respectively, and $\hat{m}$ and $\hat{b}$ represent the

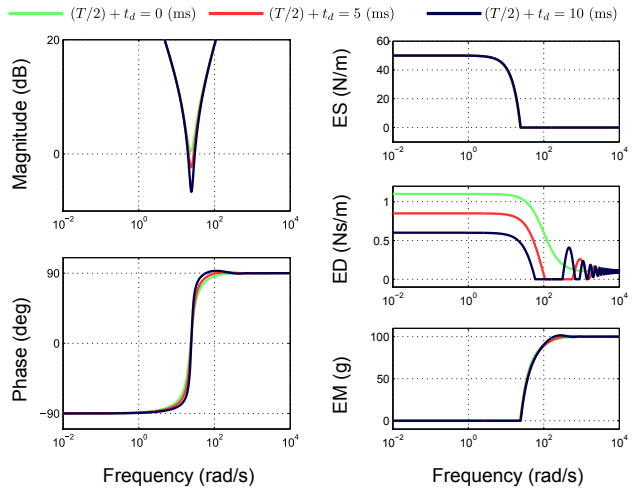

Figure 8: Spring-damper Bode and effective impedance plots with K = 50 (N/m), B = 1 (Ns/m), and varying delay. Delay reduces the ED by $K(T/2+t_d)$ at low frequencies, but does not significantly affect the ES or EM.

Figure 9: The experimental setup. Experiments were performed on a single joint of the Phantom Premium 1.5. All other joints were mechanically constrained by a custom-made "motor stop" displayed in the circle.

mass and damping of the device. The Premium was excited with an exogenous chirp force from 0.1 to 25 Hz and its position was measured. Velocity and acceleration signals were generated by numerical differentiation and smoothed with non-casual low-pass filters with no phase lag. Parameters $\hat{m}$ and $\hat{b}$ were computed from the experimental data via optimization,

$$\hat{m}_{\ell_2}, \hat{b}_{\ell_2} = \text{argmin} \sum (f_i - \hat{m}_{\ell_2}\ddot{x}_i - \hat{b}_{\ell_2}\dot{x}_i)^2, \quad (10)$$

$$\hat{m}_{\ell_1}, \hat{b}_{\ell_1} = \text{argmin} \sum |f_i - \hat{m}_{\ell_1}\ddot{x}_i - \hat{b}_{\ell_1}\dot{x}_i|, \quad (11)$$

where f_i, $\ddot{x}_i$, and $\dot{x}_i$ represent the signal values at a specific instant in time, and the subscripts ℓ_2 and ℓ_1 refer to the sum of squares and sum of absolute values objective functions, respectively. The classic pseudo-inverse was used to solve the ℓ_2 optimization problem [14]. For the ℓ_1 problem, we used CVX, a package for solving convex programs [1], [4]. Table 1 displays results averaged over five experiments for both objective functions.

4.2 Closed-loop Haptic Display Frequency Responses

To verify the theoretical predictions, we experimentally determined the frequency response of the closed-loop spring-damper haptic display with and without time delay. The parameters of the haptic display were $K = 50$ (N/m), $B = 1$ (Ns/m), and $\omega_0 = 125$ (rad/s). The external delay was implemented in software in multiples of the sample time. For each experiment, an exogenous white noise input force excited the system for two minutes at a sample rate of 1 kHz. Raw impedance ETFEs were computed by the ratio of the discrete Fourier transform (DFT) of the system's force and position [10]. The raw ETFEs were smoothed in the complex domain using a Hamming window with a length of 200 points. The theoretical results use the device parameters from the ℓ_2 objective function shown in Table 1.

Table 1: Haptic Device Fit Parameters

Objective Function	$\hat{m}$ (g)	$\hat{b}$ (Ns/m)
ℓ_2, sum of squares	94	0.10
ℓ_1, sum of absolute values	88	0.09

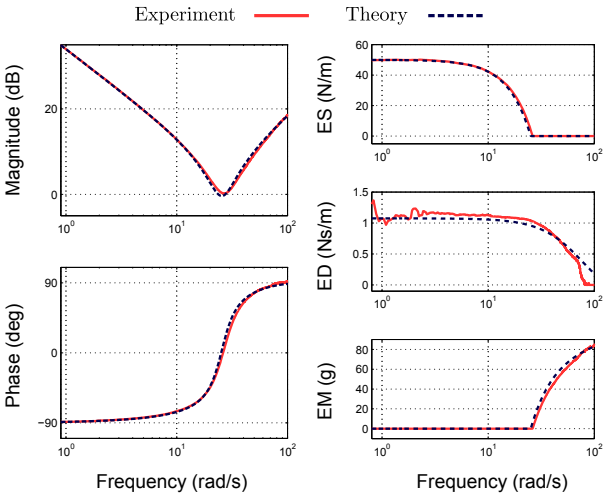

Figure 10: Experimental and theoretical bode and effective impedance plots for the closed-loop spring-damper display with no external delay. The experimental data are similar to theoretical predictions.

Figure 10 displays the experimental and theoretical Bode and effective impedance plots of the spring-damper display with no added delay. The experimental results are similar to theoretical predictions. ES is 50 (N/m) up to $\omega_s^* = 23$ (rad/s), after which it drops to zero. ED is close to the predicted value of $(b+B)$ for low frequencies, and drops near $\omega_0 = 125$ (rad/s). EM is zero up to ω_s^*, and tends to the device mass as frequency increases.

Figure 11 shows the experimental Bode and effective impedance plots of the spring-damper display with varying amounts of delay. This figure can be compared to Figure 8, which displays the corresponding theoretical results. As predicted by theory, larger delay in the control loop corresponds to a larger magnitude resonance peak at ω_s^* in the Bode plot. Time delay also reduces the ED by approximately $K(T/2+t_d)$ from its no-delay value, but does not significantly affect the ES or EM.

5 Discussion

Our results demonstrate a fundamental relationship between the system parameters given by Equation (5) and the frequency span over which the spring and spring-damper displays render an effective stiffness. This relationship informs the design of spring-type displays intending to render a stiffness. Specifically, for high effective stiffness bandwidth, large virtual spring constants and low

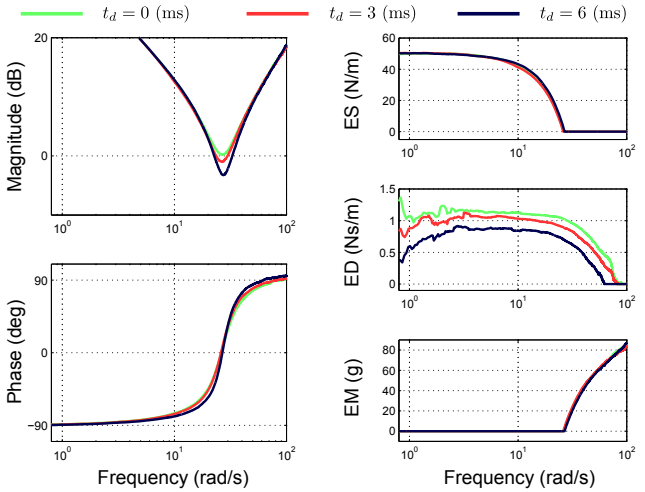

Figure 11: Experimental bode and effective impedance plots for the closed-loop spring-damper display with varying amounts of external delay. As predicted from theoretical analysis (see Figure 8), delay reduces ED by $K(T/2+t_d)$ from its no-delay value, but does not significantly affect ES or EM.

device mass are desired. Large spring constants are usually desired, but are constrained by the stability of the display [3]. The mass of most haptic devices is as small as practical to reduce open-loop inertia. Although these design objectives match conventional design, most spring-type haptic displays (with mass greater than 100 g, and maximum virtual stiffness less than 400 N/m) are necessarily low bandwidth (less than 10 Hz).

Unlike the effective stiffness bandwidth, the bandwidth of effective damping feedback in haptic displays is limited by the cut-off frequency of the low-pass filter. For many haptic displays, virtual damping is introduced to stabilize the system. If the virtual damping is too large, the damper feedback can introduce perceptible noise. Therefore, design becomes a three-way trade-off between stability, noise rejection, and accuracy.

Adding delay to spring and spring-damper displays reduces effective damping by $K(T/2+t_d)$. Similarly, adding delay reduces effective mass for damper displays by $B(T/2+t_d)$. This result demonstrates that intentionally adding delay could offset device damping or mass, however, adding delay can introduce effective jerk feedback that feels unnatural, and also has the potential to drive the system unstable.

Although time delay decreases effective damping in spring and spring-damper displays, it does not have a significant effect on the effective stiffness. These results apply when the *uncoupled* haptic display is stable (i.e., stability does not depend on human interaction). When stability does require human interaction, past research has shown that perceived stiffness is dependent on the nature of the interaction. Studies have reported that increasing delay can cause percieved stiffness to either increase [13], or decrease [7].

Future research should draw a connection between the closed-loop impedance of haptic displays and quantitative human perception. Such work will likely require human-subject experiments and a study of human physiology. In this paper, we use the concept of effective impedances to analyze accuracy. However, effective impedances are only tools to identify what *may* be important to human perception, and carry no absolute authority on the subject. Humans are able to detect haptic signals with frequencies as high as 500 Hz [6]. Volitional movement, which is especially important for active kinesthetic exploration, is limited to frequencies less than 10 Hz [9]. Understanding how the set of human mechanoreceptor signals combine to manifest haptic perception is central to designing accurate haptic displays.

6 Conclusion

Our results presented how closed-loop impedances are affected by key parameters for haptic displays with spring, damper, and spring-damper virtual environments. We presented these system impedances as sets of "effective impedances" to communicate how each display would "feel" in terms of physical analogs. We established that spring and spring-damper haptic displays render the desired effective stiffness only up to the frequency defined by Equation (5). Damper and spring-damper haptic displays render the desired effective damping up to the cut-off frequency of the low-pass filter. Time delay in the system reduces effective damping in spring and spring-damper displays, and effective mass for damper displays. Experimental data gathered with a Phantom Premium 1.5 validates this theoretical analysis. The contribution of this work facilitates the design of haptic displays by providing a theoretical framework for how system parameters affect closed-loop impedance.

Acknowledgements

This work was supported in part by National Science Foundation grant 1217635.

References

[1] S. Boyd and L. Vandenberghe. *Convex Optimization*. Cambridge University Press, New York, NY, USA, 2004.

[2] N. Diolaiti, G. Niemeyer, F. Barbagli, and J. K. Salisbury. Stability of haptic rendering: Discretization, quantization, time delay, and coulomb effects. *IEEE Transactions on Robotics*, 22(2):256–268, 2006.

[3] J. Gil, T. Hulin, C. Preusche, E. Sánchez, and G. Hirzinger. Stability boundary for haptic rendering: Influence of damping and delay. *Journal of Computing and Information Science in Engineering*, 9(1):1–8, 2009.

[4] M. Grant and S. Boyd. CVX: Matlab software for disciplined convex programming. http://cvxr.com/cvx, 2012.

[5] P. Griffiths, R. Gillespie, and J. Freudenberg. A fundamental tradeoff between performance and sensitivity within haptic rendering. *IEEE Transactions on Robotics*, 24(3):537–548, 2008.

[6] K. Hale and K. Stanney. Deriving haptic design guidelines from human physiological, psychophysical, and neurological foundations. *IEEE Computer Graphics and Applications*, 24(2):33–39, 2004.

[7] B. Knorlein, M. Di Luca, and M. Harders. Influence of visual and haptic delays on stiffness perception in augmented reality. In *IEEE International Symposium on Mixed and Augmented Reality*, pages 49–52, 2009.

[8] D. Lawrence. Stability and transparency in bilateral teleoperation. *IEEE Transactions on Robotics and Automation*, 9(5):624–637, 1993.

[9] D. Lawrence, L. Y. Pao, M. A. Salada, and A. M. Dougherty. Quantitative experimental analysis of transparency and stability in haptic interfaces. *Haptic Interfaces for Virtual Environments and Teleoperator Systems*, pages 441–449, 1996.

[10] L. Ljung. *System identification: theory for the user*. Prentice Hall, Upper Saddle River, NJ, USA, 1999.

[11] S. McJunkin, M. O'Malley, and J. Speich. Transparency of a phantom premium haptic interface for active and passive human interaction. In *Proceedings of the American Control Conference*, volume 5, pages 3060–3065, 2005.

[12] J. Mehling, J. Colgate, and M. Peshkin. Increasing the impedance range of a haptic display by adding electrical damping. In *Eurohaptics Conference*, pages 257–262, 2005.

[13] A. Pressman, L. J. Welty, A. Karniel, and F. A. Mussa-Ivaldi. Perception of delayed stiffness. *International Journal of Robotics Research*, 26(11-12):1191–1203, 2007.

[14] G. Strang. *Linear Algebra and Its Applications*. Brooks Cole, 1988.